Journal of the Mechanics and Physics of Solids 60 (2012) 1280–1295

Contents lists available at SciVerse ScienceDirect

Journal of the Mechanics and Physics of Solids

journal homepage: www.elsevier.com/locate/jmps

A finite deformation stress-dependent chemical potential and its applications to lithium ion batteries

Zhiwei Cui [a], Feng Gao [a], Jianmin Qu [a,b,*]

[a] Department of Civil and Environmental Engineering, Northwestern University, Evanston, IL 60208, USA
[b] Department of Mechanical Engineering, Northwestern University, Evanston, IL 60208, USA

ARTICLE INFO

Article history:
Received 23 July 2011
Received in revised form
18 March 2012
Accepted 24 March 2012
Available online 1 April 2012

Keywords:
Lithium-ion battery
Finite deformation
Diffusion Induced Stress (DIS)
Chemical potential
Lithiation

ABSTRACT

This paper reports the development of a new stress-dependent chemical potential for solid state diffusion under multiple driving forces including mechanical stresses. The new stress-dependent chemical potential accounts for nonlinear, inelastic, and finite deformation. By using this stress-dependent chemical potential, insertion and extraction of lithium ions into a silicon particle is investigated. The distribution and evolution of diffusion-induced stress during the insertion/extraction processes are numerically calculated. Critical particle size is obtained as a function of the charging/discharging rates. It is also found that when plastic deformation occurs, the hoop stresses on the particle surface, contrary to intuition, can become positive even during the charging process, which may explain some of the recent experimental observations.

1. Introduction

Because of the societal interest in energy storage and clean energy conversion devices, ionic transport and diffusion in various solids under electrochemical driving forces have attracted much attention in recent years. For example, Swaminathan and Qu (2007a, b, c, 2009) had investigated the diffusion-induced stress in both planar and tubular solid oxide fuel cells. Zhou et al. (2010a, b) considered the stress-oxidation interaction in selective oxidation of Cr–Fe alloys used in solid oxide fuel cells. Very recently, a number of studies have appeared on the diffusion-induced stress in silicon anode in lithium ion batteries, e.g., Sethuraman et al. (2010), Bower et al. (2011), Gao and Zhou (2011), Haftbaradaran et al. (2011), Huang and Zhu (2011) and Zhao et al. (2011a, b). In all these aforementioned works, the fundamental physics involved is the atomic or ionic diffusion in solids under multiple driving forces. Atomic diffusion in a solid may change the solid's composition from its stoichiometric state. Such a deviation from stoichiometry usually is accompanied by a volumetric change. If the volumetric change is not accommodated appropriately, it would generate a mechanical stress field in the solid, which would in turn affect the diffusion process. Such stress and diffusion interaction is governed by the thermodynamic equilibrium of the solids.

Although thermodynamic equilibrium of multi-component solids under mechanical stress has been the subject of research since Gibbs' time (Gibbs, 1906), the framework for solid state diffusion involving the change of composition while remaining in the solid state was not established until much later (Li et al., 1966; Larche and Cahn, 1973). In their seminal work, Larche and Cahn (1973) developed a thermodynamic framework for multi-component solids which reach equilibrium under non-hydrostatic stress. The framework was based on the assumption that "there exists a certain

* Corresponding author. Tel.: +1 847 467 4528.
E-mail address: j-qu@northwestern.edu (J. Qu).

0022-5096/$ - see front matter © 2012 Elsevier Ltd. All rights reserved.
http://dx.doi.org/10.1016/j.jmps.2012.03.008

identity which we shall call network which is embedded in the solid and permit the definition of a displacement and hence a strain" (Larche and Cahn, 1973). Based on this assumption, a stress-dependent chemical potential was introduced to account for the interaction between stress and diffusion. Since then, Larche and Cahn have used this general framework to solve a number of material science and engineering problems (Larche and Cahn, 1973, 1978, 1982, 1985, 1987, 1992). Recent works on the diffusion-induced stress in silicon anode in lithium ion batteries (e.g., Sethuraman et al., 2010; Bower et al., 2011; Gao and Zhou, 2011; Haftbaradaran et al., 2011; Huang and Zhu, 2011; Zhao et al., 2011a, b), have all been based on this general framework of Larche and Cahn.

In the framework of Li et al. (1966) and Larche and Cahn (1973, 1978), only the hydrostatic Cauchy stress (trace of the Cauchy stress tensor) enters the stress-dependent chemical potential. As a result, the underlying diffusion equation is actually independent of any accompanying stress field. To fully account for the two-way interaction between stress and diffusion, Wu (2001) derived a different stress-dependent chemical potential in which, instead of the hydrostatic Cauchy stress, the Eshelby momentum tensor (Eshelby, 1951, 1975) is involved. However, because of the particular approach used, the elastic moduli used in Wu's model must be those of the solid at its stoichiometry state, not at the current state.

In this paper, we present a new stress-dependent chemical potential for the finite deformation of solids. It is shown that our new stress-dependent chemical potential reduces to that of Wu (2001) if the elastic moduli are invariant to the compositional change, and to that of Larche and Cahn (1973) if both the elastic and the compositional strains are small. Comparisons among these three stress-dependent chemical potentials are made numerically by using a simple cause study.

As an example to illustrate the application of the newly developed stress-dependent chemical potential, insertion and extraction of lithium ions into a silicon particle is investigated. The distribution and evolution of diffusion-induced stress during the insertion/extraction processes are numerically calculated. Critical particle size is obtained as a function of the charging/discharging rate. It is also found that when plastic deformation occurs, the hoop stresses on the particle surface, contrary to intuition, can become positive even during the charging process.

2. Finite deformation kinematics and kinetics

The kinematics of the motion of material particles in a continuum medium can be described by a continuous displacement field $\mathbf{u}$ given by

$$\mathbf{u}=\mathbf{x}-\mathbf{X}, \tag{1}$$

where $\mathbf{x}$ is the position occupied at the current time t by the particle which occupied the position $\mathbf{X}$ in the initial configuration ($t=0$). The deformation of the continuum can be described by the deformation gradient tensors

$$F_{iJ}=\frac{\partial x_i}{\partial X_J}=\delta_{ij}+\frac{\partial u_i}{\partial X_J},\quad f_{Ij}=\frac{\partial X_I}{\partial x_j}=\delta_{Ij}-\frac{\partial u_I}{\partial x_j}. \tag{2}$$

Clearly, we have $f_{Ik}F_{kJ}=\delta_{IJ}$, where δ_{ij} is the Kronecker delta. The Lagrangian finite strain tensor is defined in terms of the deformation gradient tensor

$$E_{IJ}=\frac{1}{2}(F_{kI}F_{kJ}-\delta_{IJ})=\frac{1}{2}\left(\frac{\partial u_I}{\partial X_J}+\frac{\partial u_J}{\partial X_I}+\frac{\partial u_k}{\partial X_I}\frac{\partial u_k}{\partial X_J}\right). \tag{3}$$

The state of stress at a point in a continuum can be represented by the Cauchy stress tensor σ_{ij} in the current (or deformed) configuration. In addition to the Cauchy stress, the first and second Piola–Kirchhoff (P–K) stress may also be introduced, respectively,

$$\sigma^0_{Ij}=Jf_{Ik}\sigma_{kj},\quad \tilde{\sigma}_{IJ}=Jf_{Ik}f_{Jm}\sigma_{km}, \tag{4}$$

where $J=\det(F_{ij})$ is called the Jacobian that represents the volumetric change under the deformation F_{ij}.

The static equilibrium of the material particles requires

$$\partial\sigma^0_{Ij}/\partial X_I=0 \ \text{ or } \ \partial\sigma_{ij}/\partial x_i=0. \tag{5}$$

3. Compositional change

Without loss of generality, we consider a solid substance A_xB that consists of species A and species B. It is assumed that the concentration of A in A_xB may vary from $x=0$ to x_{max}, where x_{max} is the maximum possible concentration of A in A_xB. We note that the substance A_xB may be a crystalline or an amorphous solid. In addition, the following derivation can be easily extended to compounds with more than two species.

Furthermore, we assume that the solid in consideration can be represented by the network model of Larche and Cahn (1973). Specifically, we assume that the lattice sites of species B form a network within which species A can move (diffuse). This allows the definition of a displacement and hence a strain of the solid.

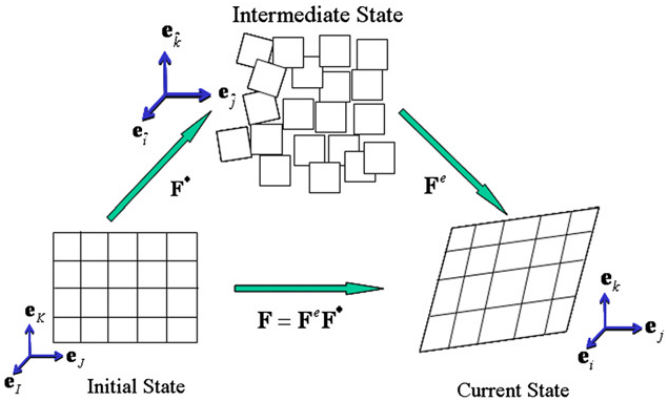

Fig. 1. Decomposition of the total deformation.

Depending upon the materials and temperature, there might be a particular value of $x=x_0$ (which could be zero) so that the solid substance A_xB is in a stress-free stoichiometric state. In this paper, we identify this stress-free stoichiometric state as the initial state, and material particles in this state will be identified by their Lagrangian coordinates **X** attached to this state.

Deviation from its stoichiometric state may cause a volumetric change (deformation) of the solid. If the change in the concentration of A is uniform throughout the solid, and the solid is not constrained mechanically, the deformation would be uniform and no stress would be generated anywhere in the solid, albeit the solid has undergone a volumetric change. Such a homogeneous deformation of the solid is inelastic since no stress is generated. Thus, it is called an eigen-transformation. However, if the solid is constrained mechanically or if the concentration is not uniform throughout the solid, stresses may be created due to the incompatibility of the eigen-transformation. In addition, plastic deformation may also occur, which can also be considered as an eigen-transformation. Consequently, elastic deformation has to occur to ensure that the total deformation is compatible. Therefore, the total deformation of the solid from its initial state may be written as

$$\mathbf{F} = \mathbf{F}^e\mathbf{F}^*, \quad \mathbf{F}^* = \mathbf{F}^c\mathbf{F}^p, \tag{6}$$

where $\mathbf{F}^c$ represents the eigen-transformation due to the compositional change, $\mathbf{F}^p$ represents the plastic deformation, and $\mathbf{F}^e$ represents the elastic deformation associated with $\mathbf{F}^*$ so that the total deformation is compatible.

Eq. (6) represents a deformation that transforms the initial (undeformed) state of the solid to its final (current or deformed) state. The total deformation can be viewed as a sequence of eigen-transformation represented by $\mathbf{F}^*$ followed by an elastic deformation represented by $\mathbf{F}^e$. The state of the solid after the eigen-transformation $\mathbf{F}^*$ is called the intermediate state. We note that the intermediate state is a stress-free state, and is not necessarily kinematically compatible. The three states of the solids are schematically shown in Fig. 1, where for clarity, the Cartesian coordinate systems $\{\mathbf{e}_I,\mathbf{e}_J,\mathbf{e}_K\}$, $\{\mathbf{e}_{\hat{i}},\mathbf{e}_{\hat{j}},\mathbf{e}_{\hat{k}}\}$, and $\{\mathbf{e}_i,\mathbf{e}_j,\mathbf{e}_k\}$ have been used in the initial, intermediate and the final (current) states, respectively.

It follows from the first of (3) that the total Lagrange strain can be written as

$$\mathbf{E} = \tfrac{1}{2}(\mathbf{F}^T\mathbf{F}-\mathbf{I}) = (\mathbf{F}^*)^T\mathbf{E}^e\mathbf{F}^* + \mathbf{E}^*, \tag{7}$$

where

$$\mathbf{E}^e = \tfrac{1}{2}[(\mathbf{F}^e)^T\mathbf{F}^e-\mathbf{I}], \quad \mathbf{E}^* = \tfrac{1}{2}[(\mathbf{F}^*)^T\mathbf{F}^*-\mathbf{I}] \tag{8}$$

can be regarded as the elastic strain and the eigenstrain, respectively.

4. Internal energy and chemical potential

Let x_0 and x_{max} be, respectively, the stoichiometric and maximum concentration of species A in A_xB. Then, the deviation from the stoichiometric concentration can be measured by $c=(x-x_0)/x_{max}$. For brevity, c will still be called the concentration in the rest of this paper without causing any confusion. If the total deformation gradient $\mathbf{F}=\mathbf{F}^e\mathbf{F}^*$ and the concentration c are taken as the independent variables, the total internal energy density per unit volume in the reference frame can be written as

$$\Pi(\mathbf{F},c) = \varphi(c)+W(\mathbf{F},c) = \varphi(c)+J^*w(\mathbf{F},c), \tag{9}$$

where $\varphi(c)$ is the internal chemical energy in the intermediate state per unit volume of the reference frame, $W(\mathbf{F},c)$ is the strain energy in the current state per unit volume of the reference frame, $w(\mathbf{F},c)$ is the strain energy per unit volume of the intermediate state, and J^* is the Jacobian that transforms an infinitesimal volume element in the initial state to the

corresponding volume in the intermediate, i.e.,

$$J^* = \det(\mathbf{F}^*). \tag{10}$$

We note that writing $W(\mathbf{F},c)$ as $J^* w(\mathbf{F},c)$ is to facilitate the derivations below. Also, for brevity, the dependence of Π on entropy and temperature is not explicitly expressed.

The chemical potential of species A per mole of species A is a thermodynamic function given by

$$\mu(\mathbf{F},c) = \frac{V_{m0}}{x_{max}}\left(\frac{\partial \Pi(\mathbf{F},c)}{\partial c}\right)_{\mathbf{F}} = \mu_0(c) + \tau(\mathbf{F},c), \tag{11}$$

where V_{m0} is the molar volume of A_xB at the stoichiometric concentration, the notation $(\partial/\partial c)_{\mathbf{F}}$ means that the partial derivative is performed while keeping $\mathbf{F}$ constant, and

$$\mu_0(c) = \frac{V_{m0}}{x_{max}}\frac{\partial \varphi(c)}{\partial c}, \quad \tau(\mathbf{F},c) = \frac{V_{m0}}{x_{max}}\left(\frac{\partial [J^* w(\mathbf{F},c)]}{\partial c}\right)_{\mathbf{F}}, \tag{12}$$

are the stress-independent and stress-dependent parts of the chemical potential, respectively.

We note that the $\mu(\mathbf{F},c)$ defined in (11) is typically not a true chemical potential. Often, it is a diffusion potential (Swaminathan et al., 2007b). The interpretation of $\mu(\mathbf{F},c)$ may differ depending upon the particular material system of interest. Nevertheless, the mathematical form is the same and the derivations below equally apply.

The stress-independent part of the chemical potential may be written as

$$\mu_0(c) = \mu_0^0 + R_g T \log(\gamma c), \tag{13}$$

where μ_0^0 is a constant that represents the chemical potential at a standard state, R_g is the standard gas constant, T is the temperature in Kelvin, and γ is the activity coefficient which represents the effects of interactions (non-ideal) among the atoms/molecules. We note that γ may also depend on c. For a dilute solution, interactions among the atoms/molecules are negligible, thus $\gamma \approx 1$.

In the remaining part of this section, we focus on carrying out the differentiation in the stress-dependent part of the chemical potential. Note that the strain energy depends not only on the deformation, but also on the stiffness $\mathbf{C}$ of the solid, which may also be a function of the concentration c. Therefore, the derivative with respect to c may be carried out in two steps, first for fixed $\mathbf{C}$, then for fixed deformation, i.e.,

$$\tau(\mathbf{F},c) = \frac{V_{m0}}{x_{max}}\left(\frac{\partial [J^* w(\mathbf{F},c)]}{\partial c}\right)_{\mathbf{F}} = \frac{V_{m0}}{x_{max}}\left[\left(\frac{\partial [J^* w(\mathbf{F},c)]}{\partial F^*_{\hat{i}J}}\frac{\partial F^*_{\hat{i}J}}{\partial c}\right)_{\mathbf{F},\mathbf{C}} + J^*\left(\frac{\partial w(\mathbf{F},c)}{\partial c}\right)_{\mathbf{F}^e,\mathbf{F}^*}\right]. \tag{14}$$

For convenience, we denote $\mathbf{f}^* = (\mathbf{F}^*)^{-1}$. Making use of the well-known relationships

$$\frac{\partial J^*}{\partial F^*_{\hat{i}J}} = \frac{\partial \det(\mathbf{F}^*)}{\partial F^*_{\hat{i}J}} = J^* f^*_{J\hat{i}}, \quad \frac{\partial f^*_{I\hat{j}}}{\partial F^*_{\hat{k}L}} = -f^*_{I\hat{k}} f^*_{L\hat{j}}, \tag{15}$$

one can show

$$\left(\frac{\partial F^e_{m\hat{n}}}{\partial F^*_{\hat{i}J}}\right)_{\mathbf{F},\mathbf{C}} = \left(\frac{\partial (F_{mK} f^*_{K\hat{n}})}{\partial F^*_{\hat{i}J}}\right)_{\mathbf{F},\mathbf{C}} = F_{mK}\frac{\partial f^*_{K\hat{n}}}{\partial F^*_{\hat{i}J}} = -F_{mK} f^*_{K\hat{i}} f^*_{J\hat{n}} = -F^e_{m\hat{i}} f^*_{J\hat{n}}. \tag{16}$$

Thus,

$$\left(\frac{\partial w(\mathbf{F},c)}{\partial F^*_{\hat{i}J}}\right)_{\mathbf{F},\mathbf{C}} = \left(\frac{\partial w(\mathbf{F},c)}{\partial F^e_{m\hat{n}}}\frac{\partial F^e_{m\hat{n}}}{\partial F^*_{\hat{i}J}}\right)_{\mathbf{F},\mathbf{C}} = -\left(\frac{\partial w(\mathbf{F},c)}{\partial F^e_{m\hat{n}}}\right)_{\mathbf{F},\mathbf{C}} F^e_{m\hat{i}} f^*_{J\hat{n}}. \tag{17}$$

Consequently,

$$\left(\frac{\partial [J^* w(\mathbf{F},c)]}{\partial F^*_{\hat{i}J}}\right)_{\mathbf{F},\mathbf{C}} = \left(\frac{\partial J^*}{\partial F^*_{\hat{i}J}}\right)_{\mathbf{F},\mathbf{C}} w(\mathbf{F},c) + J^*\left(\frac{\partial w(\mathbf{F},c)}{\partial F^*_{\hat{i}J}}\right)_{\mathbf{F},\mathbf{C}} = \Sigma_{JK} f^*_{K\hat{i}}, \tag{18}$$

where

$$\Sigma_{JK} = \delta_{JK} W(\mathbf{F},c) - J^*\left(\frac{\partial w(\mathbf{F},c)}{\partial F^e_{m\hat{n}}}\right)_{\mathbf{F},\mathbf{C}} F_{mK} f^*_{J\hat{n}} \tag{19}$$

can be called the generalized Eshelby stress tensor in that for hyperelastic materials

$$\frac{\partial w(\mathbf{F},c)}{\partial F^e_{m\hat{n}}} = \frac{1}{J^*} F^*_{\hat{n}K} \sigma^0_{Km} \tag{20}$$

which leads to the conventional Eshelby stress tensor (Eshelby, 1951, 1975)

$$\Sigma_{JK} = [\delta_{JK} W(\mathbf{F},c) - \sigma^0_{Jm} F_{mK}]. \tag{21}$$

It is not surprising that the Eshelby stress tensor naturally appears in the stress-dependent chemical potential. In fact, as pointed out in Cleja-Tigoiu and Maugin (2000) that the Eshelby stress tensor often arises in problems involving compositional/microstructural changes, because the Eshelby stress tensor provides a stress measure in the elastically released intermediate configuration.

The appearance of the Eshelby stress brings the elastic energy into the chemical potential. Thus, the interplay between a composition-generated deformation and another elastic field may become important via the interaction energy. This marks the fundamental difference between the current model and the model of Larche and Cahn (1973, 1978). Further discussions of this difference can be found in Wu (2001).

In conjunction with the first of (4), one can easily show that

$$\Sigma_{KK} = [3W(\mathbf{F},c) - \sigma^0_{Km}F_{mK}] = 3W(\mathbf{F},c) - J\sigma_{kk}. \tag{22}$$

Finally, substituting (18) into (14) gives the stress-dependent part of the chemical potential

$$\tau(\mathbf{F},c) = \frac{V_{m0}}{x_{max}}\left[\Sigma_{JK}f^*_{K\hat{i}}\left(\frac{\partial F^*_{\hat{i}J}}{\partial c}\right)_{\mathbf{F},\mathbf{C}} + J^*\left(\frac{\partial w(\mathbf{F},c)}{\partial c}\right)_{\mathbf{F}^e,\mathbf{F}^*}\right]. \tag{23}$$

Further, if the material is linearly elastic, one has

$$W(\mathbf{F},c) = J^c w(\mathbf{F},c), \quad w(\mathbf{F},c) = \tfrac{1}{2}C_{\hat{i}\hat{j}\hat{k}\hat{l}}E^e_{\hat{i}\hat{j}}E^e_{\hat{k}\hat{l}}, \tag{24}$$

where $C_{\hat{i}\hat{j}\hat{k}\hat{l}}$ is the elasticity tensor of the material in the intermediate state, which may depend on the concentration c. In this case, (23) can be cast into a form that is more convenient to use

$$\tau(\mathbf{F},c) = \frac{V_{m0}}{x_{max}}\left[-\frac{1}{3}\frac{\partial J^c}{\partial c}F^e_{\hat{i}\hat{m}}F^e_{\hat{i}\hat{n}}C_{\hat{m}\hat{n}\hat{k}\hat{l}}E^e_{\hat{k}\hat{l}} + \frac{1}{2}\left(J^c\frac{\partial C_{\hat{i}\hat{j}\hat{k}\hat{l}}}{\partial c} + \frac{\partial J^c}{\partial c}C_{\hat{i}\hat{j}\hat{k}\hat{l}}\right)E^e_{\hat{i}\hat{j}}E^e_{\hat{k}\hat{l}}\right]. \tag{25}$$

Clearly, three terms of right side of (25) represent the chemical potential contributions from first Piola–Kirchhoff stress tensor, varying elastic modulus and elastic strain energy, respectively.

5. Special cases

In the rest of this paper, we assume. First, note that for hyperelastic materials under elastic deformation with isotropic eigen-transformation $\mathbf{F}^c = (J^c)^{1/3}\mathbf{I}$, (23) reduces to

$$\tau(\mathbf{F},c) = V^B_m\left[\frac{\eta}{J^c}\Sigma_{KK} + \frac{J^c}{x_{max}}\left(\frac{\partial w(\mathbf{F},c)}{\partial c}\right)_{\mathbf{F}^e,\mathbf{F}^c}\right]. \tag{26}$$

where $J^c = 1+3\eta x_{max}c$ and V^B_m is the molar volume of species B in the initial state. η is the coefficient of compositional expansion (CCE), which is a material property that characterizes the linear measure of the volumetric change due to unit change of the concentration (Swaminathan et al., 2007c). For a given material, the CCE can be obtained either experimentally, or by conducting molecular dynamic simulations (Swaminathan and Qu, 2009; Cui et al., 2011).

It is noted that, although the form of (26) is similar to that of Wu (2001), there is a significant difference between these two results. The elasticity tensor $\mathbf{C}(c)$ appeared in (26) is evaluated at the current concentration c, while in Wu (2001) the elasticity tensor is evaluated at the stoichiometric concentration. In other words, when explicitly written, Wu's result is actually

$$\tau(\mathbf{F},c) = V^B_m\left[\frac{\eta}{J^c}\Sigma_{KK}\,|_{c=0} + \frac{J^c}{x_{max}}\left(\frac{\partial w(\mathbf{F},c)}{\partial c}\Big|_{c=0}\right)_{\mathbf{F}^e,\mathbf{F}^c}\right]. \tag{27}$$

Clearly, the difference between (26) and (27) becomes negligible when the concentration deviates slightly from stoichiometry and/or the elastic modulus does not change significantly with respect to the concentration. In fact, these were the assumptions implicitly used in Wu (2001). These assumptions are necessary because of the particular method used in Wu (2001) to derive (27).

Next, again consider isotropic eigen-transformation $\mathbf{F}^c = (J^c)^{1/3}\mathbf{I}$, $J^c = 1+3\eta x_{max}c$. Further, assume that the deformation is linearly elastic, and both the elastic strain and the eigenstrain are small so that terms of order $\boldsymbol{\sigma}^0\mathbf{E}^e$ or higher can be neglected and $J^c \approx 1$. Under these assumptions, one can show that (23) reduces to

$$\tau(\mathbf{F},c) = \frac{V^B_m}{x_{max}}\left[-\frac{\sigma_{kk}}{3}\frac{\partial J^c}{\partial c} + \frac{1}{2}\frac{\partial C_{\hat{i}\hat{j}\hat{k}\hat{l}}(c)}{\partial c}E^e_{\hat{i}\hat{j}}E^e_{\hat{k}\hat{l}}\right]. \tag{28}$$

This is identical to the result given by Larche and Cahn (1973). In other words, the result of Larche and Cahn (1973) is valid only when both elastic strain and eigenstrain are small. For some problem, the eigenstrain may not be small. For example, insertion of lithium into silicon can induce as much as 400% volume change. Clearly, J^c can be significantly different from unity.

To compare the different levels of simplifications and their validity, we consider an idealized example in this section. Imagine a spherical particle made of one mole of amorphous silicon (Si) atoms. For simplicity, we assume that particle is encased within a rigid shell so that its volume cannot expand, as shown in Fig. 2. Next, assume that x moles of lithium (Li) are inserted into the particle so that the concentration of Li in the Li_xSi is $c=(x/x_{max})$, where for Si, $x_{max}=4.4$. Further, we assume that Li is uniformly distributed throughout the spherical particle. Clearly, this is an extremely idealized example. But, it will serve our purpose.

Under these assumptions, it is obvious that $\mathbf{F}=\mathbf{I}$ and $\mathbf{F}^p=\mathbf{I}$. Thus, one can easily write down the following:

$$\mathbf{F}^c=(J^c)^{1/3}\mathbf{I},\quad \mathbf{F}^e=(J^c)^{-1/3}\mathbf{I},\quad \mathbf{E}^e=\tfrac{1}{2}\left[(J^c)^{-2/3}-1\right]\mathbf{I}. \tag{29}$$

We further assume that the Li_xSi alloy is isotropic and linearly elastic, i.e.,

$$W(\mathbf{F},c)=\frac{J^c}{2}\frac{E(c)}{(1+\nu)}\left(\frac{\nu}{1-2\nu}(E^e_{\hat{k}\hat{k}})^2+E^e_{\hat{j}\hat{k}}E^e_{\hat{k}\hat{j}}\right), \tag{30}$$

where Poisson's ratio ν is independent of c and Young's modulus is given by

$$E(c)=E(0)[1+\eta_E x_{max}c]. \tag{31}$$

The constant η_E is the intrinsic material property that characterizes the variation of Young's modulus with respect to Li concentration c. Combining (29) and (30) leads to

$$W(\mathbf{F},c)=\frac{3E(c)J^c}{8(1-2\nu)}[(J^c)^{-2/3}-1]^2. \tag{32}$$

For Li_xSi under elastic deformation, the compositional expansion may be written as $J^c=1+3\eta x_{max}c$.

Making use of the above, the stress-dependent part of the chemical potential can be evaluated from (26)–(28). Shown in Fig. 3 is the comparison among these different formulas versus c. The parameters used in the calculations are tabulated

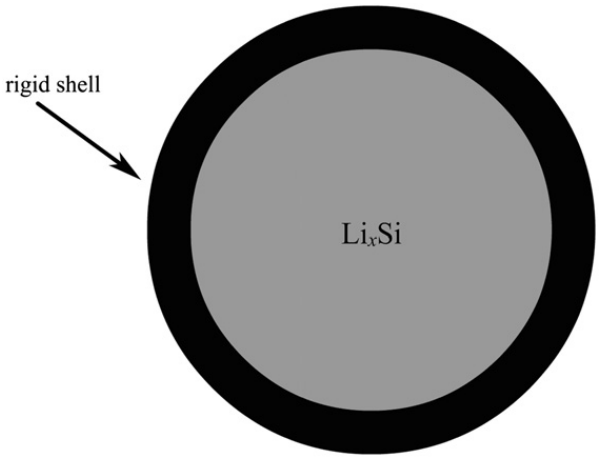

Fig. 2. Illustration of spherical particle with a rigid shell.

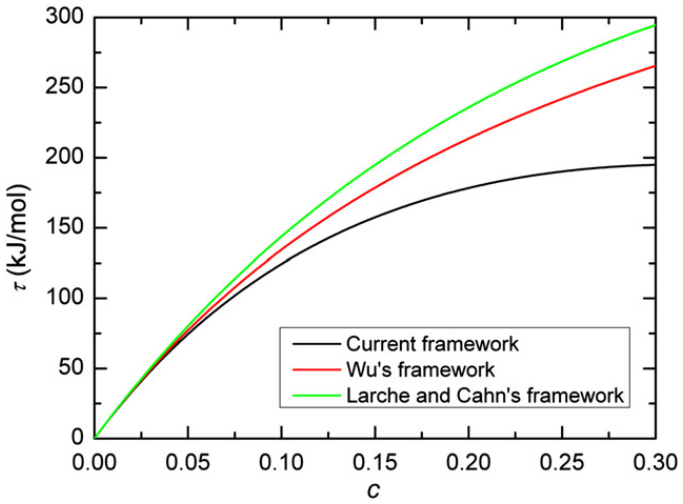

Fig. 3. $\tau(\mathbf{F},c)$ vs. c computed from (26) (this paper), (27) (Wu, 2001), and (28) (Larche and Cahn, 1973), respectively.

Table 1
Material properties and initial parameters used in our model.

A_0, parameters of the activity constant	-0.3063 eV/atom
B_0, parameters of the activity constant	-0.4003 eV/atom
D_0, diffusivity of Si anode	1×10^{-16} m^2/s[a]
$\dot{d}_0$, characteristic strain rate for plastic flow in Si	1×10^{-3} s^{-1}
E_0, elastic constant of pure silicon	90.13 GPa[b]
m, stress exponent for plastic flow in Si	4[c]
R_g, gas constant	8.314 J K^{-1} mol^{-1}
R_0, initial radius of unlithiated Si anode	200 nm
T, temperature	300 K
V_m^B, molar volume of Si	1.2052×10^{-5} m^3/mol
x_{max}, maximum concentration	4.4
α, coefficient of diffusivity	0.18[d]
η, coefficient of compositional expansion (CCE)	0.2356
η_E, rate of change of elastic modulus with concentration	-0.1464[b]
ν_0, Poisson's ratio of Si electrode	0.28
σ_f, initial yield stress of Si	0.12 GPa[c]

[a] Liu et al. (2011).
[b] Rhodes et al. (2010).
[c] Bower et al. (2011).
[d] Haftbaradaran et al. (2011).

in Table 1. It is seen that for c less than 10%, these three formulas give very similar results. The results are different for larger concentrations (i.e., larger eigenstrains) or larger elastic strains.

6. Spherical silicon particle

As an example to illustrate the use of the newly developed stress-dependent chemical potential, we consider a spherical amorphous silicon (Si) particle of initial radius R_0 (anode). Let the particle be immersed in a liquid electrolyte of infinite extent containing lithium ions of sufficient concentration. Further, by neglecting the hydrostatic pressure in the liquid electrolyte, the particle surface can be considered traction-free. Thus, the problem is spherically symmetric, i.e., in the spherical coordinate system (R,Θ,Φ), the displacement field inside the Si particle can be written as

$$u_R = u(R,t), \quad u_\Theta = u_\Phi = 0. \tag{33}$$

The traction-free boundary condition is thus expressed as

$$\sigma_R(R_0,t) = \sigma_{R\Theta}(R_0,t) = \sigma_{R\Phi}(R_0,t) = 0. \tag{34}$$

During lithium insertion, the boundary condition for the Li flux at the surface can be written as

$$J_R(R_0,t) = J_0[1-c(R_0,t)], \quad J_\Theta(R_0,t) = J_\Phi(R_0,t) = 0, \tag{35}$$

where J_0 is a constant representing the charging rate. It can be shown that (35) is a linearized form of the Butler–Volmer equation (Chen et al., 2009). Upon discharging (lithium extraction), the boundary condition for the Li flux at the surface should be changed to

$$J_R(R_0,t) = -J_0 c(R_0,t), \quad J_\Theta(R_0,t) = J_\Phi(R_0,t) = 0, \tag{36}$$

Further, we assume that the lithiated state (Li_xSi) remains amorphous so that its elastic properties are linear and isotropic before plastic yielding occurs, and can be represented by Young's modulus and Poisson's ratio

$$E(c) = E_0(1+\eta_E x_{max} c), \quad \nu = \nu_0, \tag{37}$$

where E_0 and ν_0 are the elastic properties of pure amorphous Si. The constant η_E represents the variation of Young's modulus with respect to Li concentration c.

Finally, assume that the eigen-transformation during lithiation is isotropic and given by

$$\mathbf{F}^c = (J^c)^{1/3}\mathbf{I}, \quad J^c = 1+3\eta x_{max} c, \tag{38}$$

where $x_{max} = 4.4$ represents the saturation of Li in Li_xSi, and η is the CCE (Swaminathan et al., 2007b).

We are now ready to derive the governing equations for the insertion/extract process. First, symmetry of the problem dictates that the deformation is

$$\mathbf{F} = \langle F_{11}, F_{22}, F_{33}\rangle = \langle 1+\partial u/\partial R, 1+u/R, 1+u/R\rangle, \tag{39}$$

where the brackets stands for the diagonal of a matrix. If the plastic deformation is incompressible, i.e., $\det(\mathbf{F}^p) = 1$, one can write

$$\mathbf{F}^p = \langle \lambda_p, 1/\sqrt{\lambda_p}, 1/\sqrt{\lambda_p}\rangle, \tag{40}$$

where λ_p is the plastic stretch in the radial direction. Combining (38) and (39) leads to

$$\mathbf{F}^e = \langle F_R^e, F_\Theta^e, F_\Phi^e \rangle = (J^c)^{-1/3} \left\langle \frac{1+\partial u/\partial R}{\lambda_p}, (1+u/R)\sqrt{\lambda_p}, (1+u/R)\sqrt{\lambda_p} \right\rangle, \tag{41}$$

where $F_\Theta^e = F_\Phi^e$ due to symmetry. Clearly, there are three unknowns, i.e., u, c and λ_p. Making use of (41) in (8) gives the elastic strain

$$\mathbf{E}^e = \tfrac{1}{2}[(\mathbf{F}^e)^T\mathbf{F}^e - \mathbf{I}] = \langle E_R^e, E_\Theta^e, E_\Theta^e \rangle. \tag{42}$$

Let the elastic behavior be defined by the strain energy density in the reference frame

$$W(\mathbf{F},c) = \frac{J^c}{2}\frac{E(c)}{(1+\nu)}\left(\frac{\nu}{1-2\nu}(E_{kk}^e)^2 + E_{jk}^e E_{kj}^e\right). \tag{43}$$

The strain energy density in the intermediate state is simply $w(\mathbf{F},c) = (W(\mathbf{F},c)/J^c)$. The first P–K stress can then be computed from (43) using (20). For the particular case considered here, it can be shown that the non-zero components of the first P–K stress tensor are given, respectively, by

$$\sigma_R^0 = \frac{J^c E(c)}{(1+\nu)(1-2\nu)}\left[(1-\nu)E_R^e + 2\nu E_\Theta^e\right]\frac{2E_R^e+1}{1+\partial u/\partial R}, \tag{44}$$

$$\sigma_\Theta^0 = \sigma_\Phi^0 = \frac{J^c E(c)}{(1+\nu)(1-2\nu)}(\nu E_R^e + E_\Theta^e)\frac{2E_\Theta^e+1}{1+u/R}. \tag{45}$$

In deriving (44) and (45), $\mathbf{F}^e\mathbf{F}^c\mathbf{F}^p = \mathbf{F}$ has been used. The corresponding Cauchy stresses are given by

$$\sigma_R = \frac{E(c)}{(1+\nu)(1-2\nu)}\left[(1-\nu)E_R^e + 2\nu E_\Theta^e\right]\frac{\sqrt{1+2E_R^e}}{1+2E_\Theta^e}, \tag{46}$$

$$\sigma_\Theta = \sigma_\Phi = \frac{E(c)}{(1+\nu)(1-2\nu)}(\nu E_R^e + E_\Theta^e)\frac{1}{\sqrt{1+2E_R^e}}. \tag{47}$$

To describe the plastic behavior, we first consider the rate of plastic deformation tensor

$$\mathbf{D}^p = \tfrac{1}{2}[(\mathbf{L}^p)^T + \mathbf{L}^p], \tag{48}$$

where $\mathbf{L}^p$ is the plastic part of the spatial gradient of the velocity

$$\mathbf{L}^p \equiv \mathbf{F}^e\mathbf{F}^c\dot{\mathbf{F}}^p(\mathbf{F}^p)^{-1}(\mathbf{F}^c)^{-1}(\mathbf{F}^e)^{-1}. \tag{49}$$

Since all three deformation gradient tensors are diagonal in the particular case considered here, the rate of plastic deformation is simplified to

$$\mathbf{D}^p = \dot{\mathbf{F}}^p(\mathbf{F}^p)^{-1} = \frac{\dot{\lambda}_p}{2\lambda_p}\langle 2,-1,-1\rangle. \tag{50}$$

Next, consider the deviatoric part of the Cauchy stress

$$\boldsymbol{\tau} = \boldsymbol{\sigma} - \frac{\sigma_{kk}}{3}\mathbf{I} = \frac{\sigma_R - \sigma_\Theta}{3}\langle 2,-1,-1\rangle. \tag{51}$$

The corresponding effective stress is then given by

$$\sigma_{eff} = \sqrt{\frac{3}{2}}\sqrt{\tau_{ij}\tau_{ij}} = |\sigma_R - \sigma_\Theta|. \tag{52}$$

Finally, the viscoplastic behavior of Li_xSi can be described by the following constitutive equation:

$$\mathbf{D}^p = \frac{\partial G(\sigma_{eff})}{\partial \boldsymbol{\tau}}, \tag{53}$$

where $G(\sigma_{eff})$ is the flow potential. Following Bower et al. (2011), we adopt the following power-law form for the flow potential:

$$G(\sigma_{eff}) = \frac{\sigma_f \dot{d}_0}{m+1}\left(\frac{\sigma_{eff}}{\sigma_f} - 1\right)^{m+1} H\left(\frac{\sigma_{eff}}{\sigma_f} - 1\right), \tag{54}$$

where $H(x)$ is the Heaviside step function, σ_f, $\dot{d}_0$ and m are material constants, which may depend on the Li concentration. Clearly, σ_f is the unidirectional yield (Cauchy) strength, $\dot{d}_0$ is the reciprocal of viscosity and m is the stress exponent ($m=1$ yields viscoelastic behavior). We note that this is a slightly modified version of the one used by Bower et al. (2011). The modification is to ensure a smooth transition from the elastic to the plastic regimes. The material constants σ_f, $\dot{d}_0$ and m used in the numerical simulations are listed in Table 1.

Making use of (54) in (53), and carrying out the derivative lead to

$$\mathbf{D}^p = \mathrm{sgn}(\sigma_R - \sigma_\Theta)\frac{\dot{d}_0}{2}\left(\frac{\sigma_{eff}}{\sigma_f}-1\right)^m \langle 2,-1,-1\rangle H\left(\frac{\sigma_{eff}}{\sigma_f}-1\right), \tag{55}$$

where sgn(x) is the Sign function. Combining (50) and (55) yields

$$\frac{\dot{\lambda}_p}{\lambda_p} = \mathrm{sgn}(\sigma_R - \sigma_\Theta)\dot{d}_0\left(\frac{\sigma_{eff}}{\sigma_f}-1\right)^m H\left(\frac{\sigma_{eff}}{\sigma_f}-1\right). \tag{56}$$

This is effectively the constitutive law governing the viscoplastic deformation of the Li_xSi particle.

Other equations governing the insertion/extraction process include the only non-trivial mechanical equilibrium equation

$$\frac{\partial \sigma_R^0}{\partial R} + 2\frac{\sigma_R^0 - \sigma_\Theta^0}{R} = 0, \tag{57}$$

and the only non-trivial continuity equation

$$\frac{\partial c}{V_m^B \partial t} + \frac{\partial J_R}{\partial R} + \frac{2J_R}{R} = 0. \tag{58}$$

where

$$J_R = -\frac{D}{R_g T}\frac{c}{V_m^B}\frac{\partial \mu(\mathbf{F},c)}{\partial R}, \tag{59}$$

is the only non-zero component of the Li flux, D is the diffusivity, which may be stress and concentration dependent.

It can be shown that by using the elastic constitutive equations and the kinematic equations, the stresses, the elastic strains and the chemical potential can all be expressed as functions of three independent variables, namely Li concentration c, radial displacement u, and the radial plastic stretch λ_p, all of which are functions of R and t. Therefore, (56)–(58) form a system of three nonlinear partial differential equations (PDEs). The boundary conditions for these PDEs are given by (34) and (35) for insertion and (36) for extraction. In addition, initial conditions are needed, which can be specified by

$$c(R,0) = 0, \quad u(R,0) = 0, \quad \lambda_p(R,0) = 1 \tag{60}$$

These define a boundary/initial value problem that can be solved to obtain c, u, and λ_p. Once c, u, and λ_p are known as function of R and t, other field quantities can be computed. For example, the stress σ_R and σ_Θ can be obtained from (46) and (47).

The above boundary/initial value problem does not seem to admit an analytical solution. It is solved numerically in this study by using the COMSOL multiphysics software. In our numerical calculations, the activity constant and the diffusivity are assumed to depend on Li concentration according to the followings (Haftbaradaran et al., 2011):

$$\gamma = \frac{1}{1-c}\exp\left(\frac{1}{R_g T}\left[2(A_0 - 2B_0)c - 3(A_0 - B_0)c^2\right]\right), \tag{61}$$

$$D = D_0\tilde{D} \equiv D_0 \exp\left(\frac{\alpha V_m^B \sigma_\Theta^0}{R_g T}\right). \tag{62}$$

The values of A_0 and B_0 can also be derived from the mixing enthalpy of Li_xSi by using first-principles calculations (Shenoy et al., 2010). The constants in the above and other materials properties used in the numerical calculations are given in Table 1.

For convenience, the following non-dimensional parameters are introduced in the numerical solution

$$\tilde{R} = \frac{R}{R_0}, \quad \tilde{D} = \frac{D}{D_0}, \quad \tilde{t} = \frac{D_0 t}{R_0^2}, \quad \tilde{u} = \frac{u}{R_0}, \quad \tilde{J}_R = \frac{V_m^B R_0 J_R}{D_0}, \quad \tilde{J}_0 = \frac{V_m^B R_0 J_0}{D_0}. \tag{63}$$

The numerical results presented here are all in terms of these non-dimensional parameters.

Let us first consider the cases where plastic deformation does not occur. Shown in Fig. 4 is the Li concentration distribution along the radial direction at different times and under various charging rates. It is seen that within the charging rate considered here, $10^{-3} \le \tilde{J}_0 \le 10^{-1}$, the concentration is rather uniform over the particle, even at very early times. At later times (not shown) the concentration becomes almost uniform. To generate large distribution gradient, higher charging rates are needed, which would generate extremely high stress.

The stress distribution corresponding to the cases shown in Fig. 4 is presented in Fig. 5. It is seen that the stresses are rather non-uniform along the radial direction, although the Li concentration is relatively uniform (see Fig. 4). Furthermore, even for a few percent of Li concentration, the stress can be as high as several hundreds of MPa. The results for the hoop stress σ_Θ also show that it is tensile in the inner core, and compressive in the outer shell. Intuitively, this seems to make sense since Li has higher concentration in the outer shell as indicated in Fig. 4.

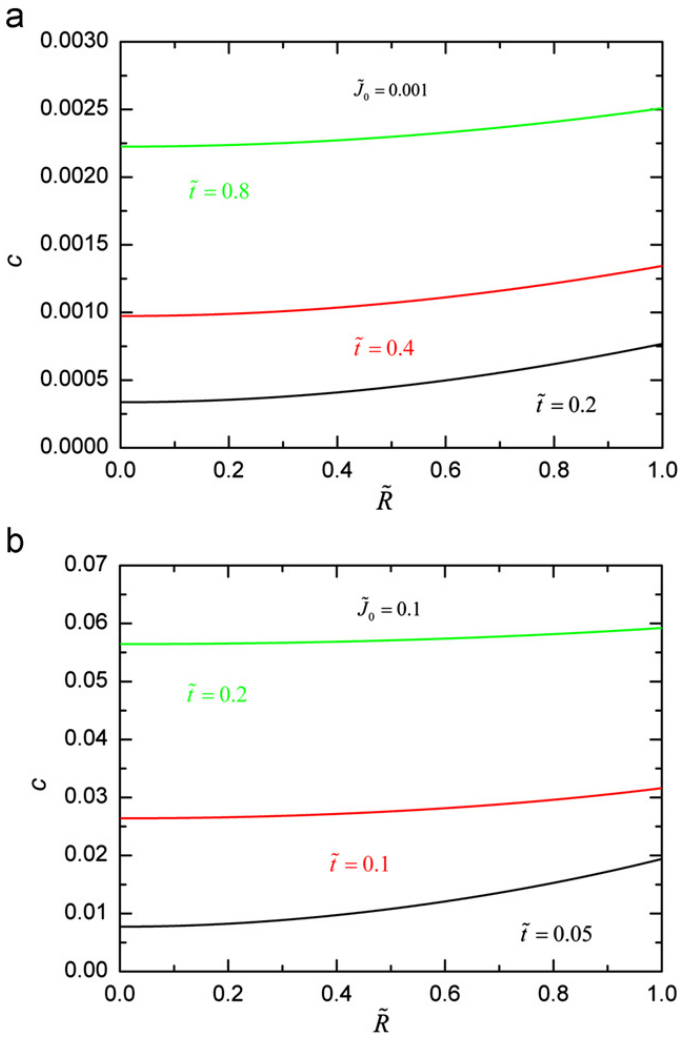

Fig. 4. Li concentration distributions at different times and under different charging rates.

The evolution of stresses at the center and at a point on the particle surface is plotted in Fig. 6 under different charging rates. One obvious observation is that stresses reach their maximum at the very beginning of charging, and decreases dramatically afterwards, and eventually vanishes at full charge (not shown). The maximum stress increases monotonically with increasing charging rate. In particular, we note that the hoop stress on the outer surface is always negative, or the outer shell of the particle is always under compression. As will be seen later, this is not the case when plasticity is considered.

Fig. 7 provides a perspective of the non-dimensional charging rates used in the above calculations, where the Li concentration or capacity is plotted as a function of $\tilde{t}\tilde{J}_0$. First, it is rather interesting that all the data fall onto a single line, indicating that charging time and charging rate are reciprocal. In other words, double the charging rate would reduce the time to full charge by half. Second, the curve shows that the time to full charge depends on the charging rate $\tilde{J}_0$. For $10^{-3} \le \tilde{J}_0 \le 10^{-1}$, the time to full charge is between $20 \le \tilde{t} \le 2 \times 10^3$. Since $\tilde{t} = (D_0 t/R_0^2)$, one needs to know the diffusivity and the particle radius in order to convert $\tilde{t}$ to real time. For example, for $R_0 = 100$ nm, $D_0 = 10^{-16}$ m^2/s, the real time corresponding to the above range of dimensionless time is between 33 min and 55 h. Fig. 7 also shows that charging gets harder at higher capacity. For example, the figure shows that charging the anode to 90% capacity takes only about half the time needed to fully charge it.

It is well known that the large stress induced by Li insertion may damage the Si anode during charging and discharging (e.g., Cheng and Verbrugge, 2010). Damage is most likely to occur when the Si particle is greater than a critical size (e.g., Kim et al., 2011). This critical particle size can be estimated based on the fact that our numerical results show that the maximum stress σ_{max} is a power-law function of the dimensionless charging rate $\tilde{J}_0$, i.e., $\sigma_{max} = A(\tilde{J}_0)^{1/n}$, where A and n are constants depending on the material properties, the anode geometry, and how the maximum stress is defined. It then follows the definition of $\tilde{J}_0$ that the critical radius for damage initiation is given by

$$R_c = \frac{D_0 \tilde{J}_{0c}}{J_0 V_m} = \frac{B D_0}{J_0 V_m} \left(\frac{\sigma_c}{E_0}\right)^n, \tag{64}$$

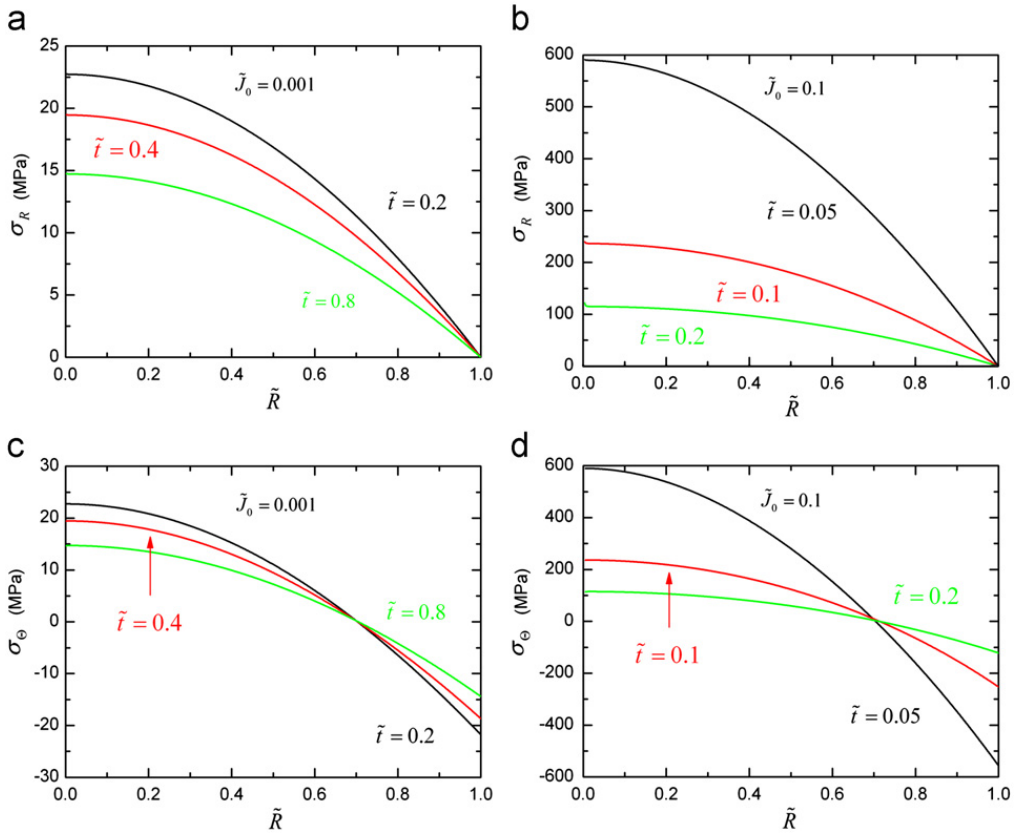

Fig. 5. Stress distribution at different times under various changing rates.

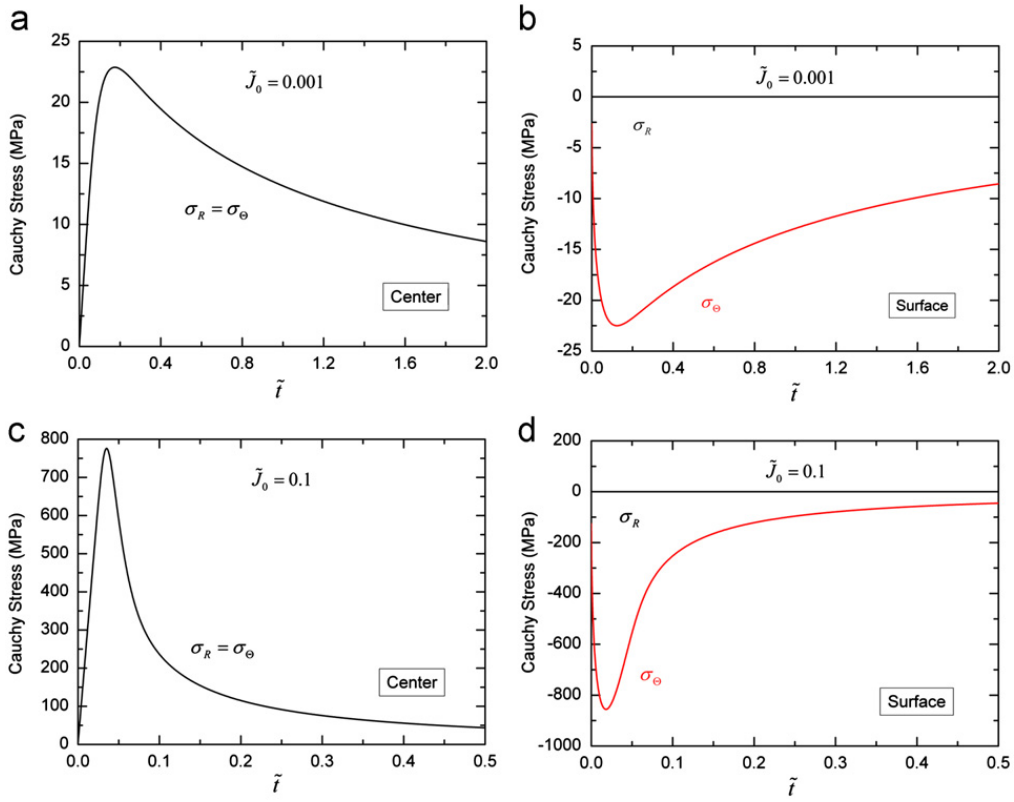

Fig. 6. Evolution of stresses at the center and at a point on the surface of the particle.

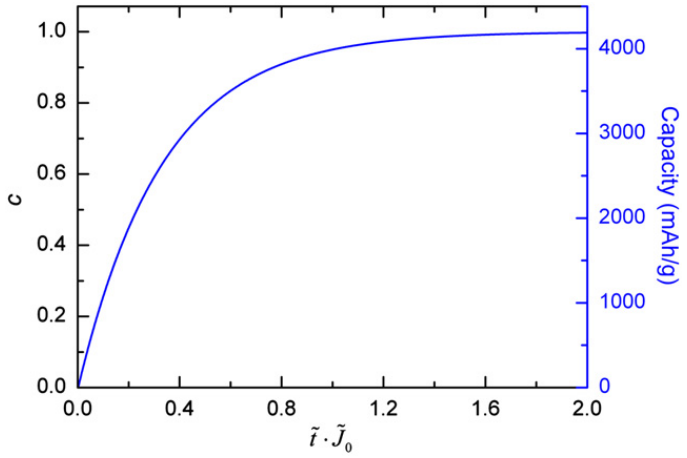

Fig. 7. Li concentration (or charge capacity) versus charging time under a given charging rate, or Li concentration versus charging rate for a given charging time.

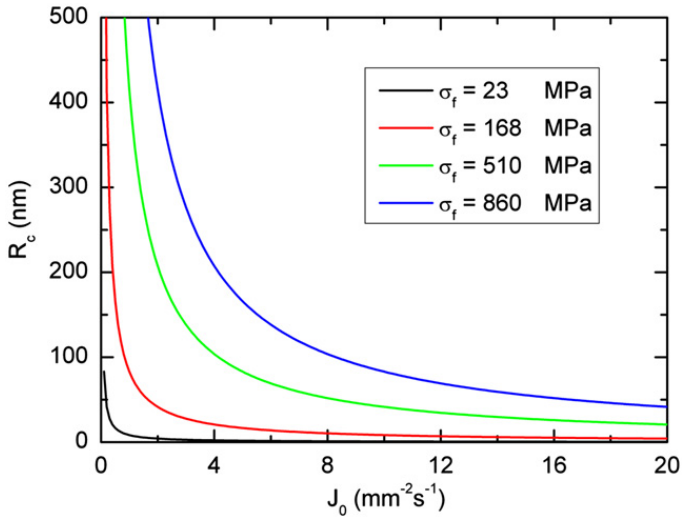

Fig. 8. Critical particle size against plastic deformation as a function of charging rate.

where σ_c is the critical stress (a material property) at which damage occurs, and B is dimensionless constants that may depend on the material properties, the anode geometry, and the particular failure criterion used. For example, if $\sigma_{max} = \max\{\sigma_{eff}\} = \sigma_c = \sigma_f$, where σ_f is the yield strength and σ_{eff} is given in (52), is used as a failure criterion, the constants for a spherical particle will be $B=35$ and $n=1.3$.

Eq. (64) shows that the critical particle size R_c inversely depends on the charging rate J_0. Plotted in Fig. 8 are the R_c vs. J_0 curves for several different values of σ_c. For a given charging rate, one can identify the critical particle size beyond which damage would occur. Similarly, one can also find the time needed to charge a particle at the highest possible charging rate without causing damage. This information is shown in Fig. 9, where the time to 80% of full charge is plotted as a function of the maximum possible charging rate without causing damage (plastic yielding in this case) for various yield strengths of the Li_xSi alloy.

To compare with available experimental data in the open literature, we have also carried out the same computations and analyses for a Si wire anode. Without showing all the results, we only mention that, using the parameters in Table 1, we found that $B=18$, and $n=1.2$ for the Si wire anode. The critical wire diameter predicted by (64) is about 220 nm when the charging rate is $C/10$ (i.e., the anode is fully charged in 10 h). This is in good agreement with the experimental observations under the same charging rate (Teki et al., 2009).

When plastic deformation is allowed, not only the magnitude of the stress is reduced due to yielding, the distribution of stresses is also altered significantly. As Fig. 10 shows, the radial stress is positive at early charging stage, and gradually becomes negative throughout the particle after certain charging time. More remarkably, the hoop stress, in the beginning, is positive inside and negative near the surface, i.e., the surface is under compression. As charging progresses, the sign switches, i.e., the hoop stress gradually becomes negative inside the particle, and positive near the surface, indicating that the particle surface will be subjected to tensile hoop stress at some point during charging.

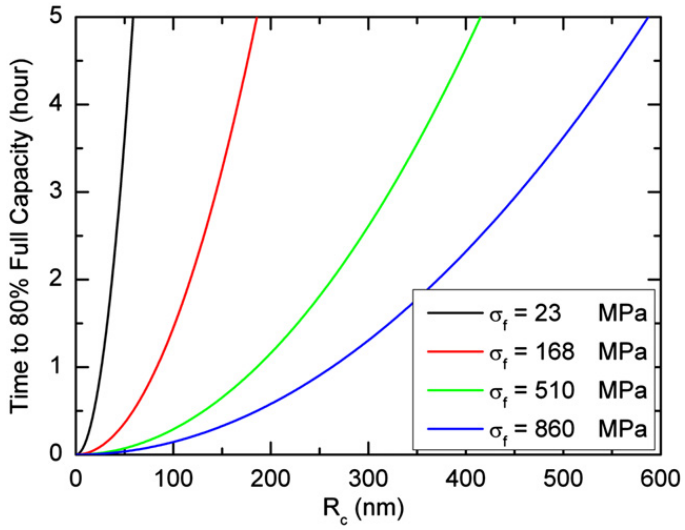

Fig. 9. The time needed to reach 80% of full charge by using a maximum possible charging rate without causing plastic yielding.

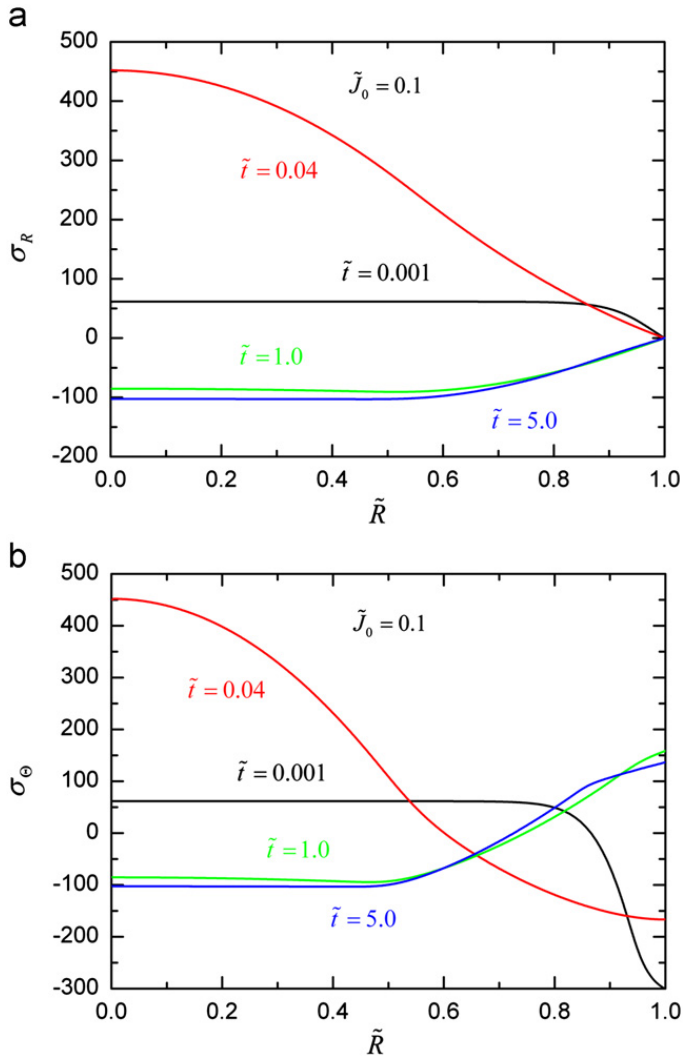

Fig. 10. Stress distribution when plastic deformation is allowed.

To better visualize the evolution of the hoop stress, Fig. 11 plots the hoop stress at the center and at a point on the particle surface as a function of time. It is seen that, at the center, the hoop stress (which equals the radial stress at the center) starts from zero, raises to a positive maximum, then decreases gradually to a negative value. On the surface, hoop

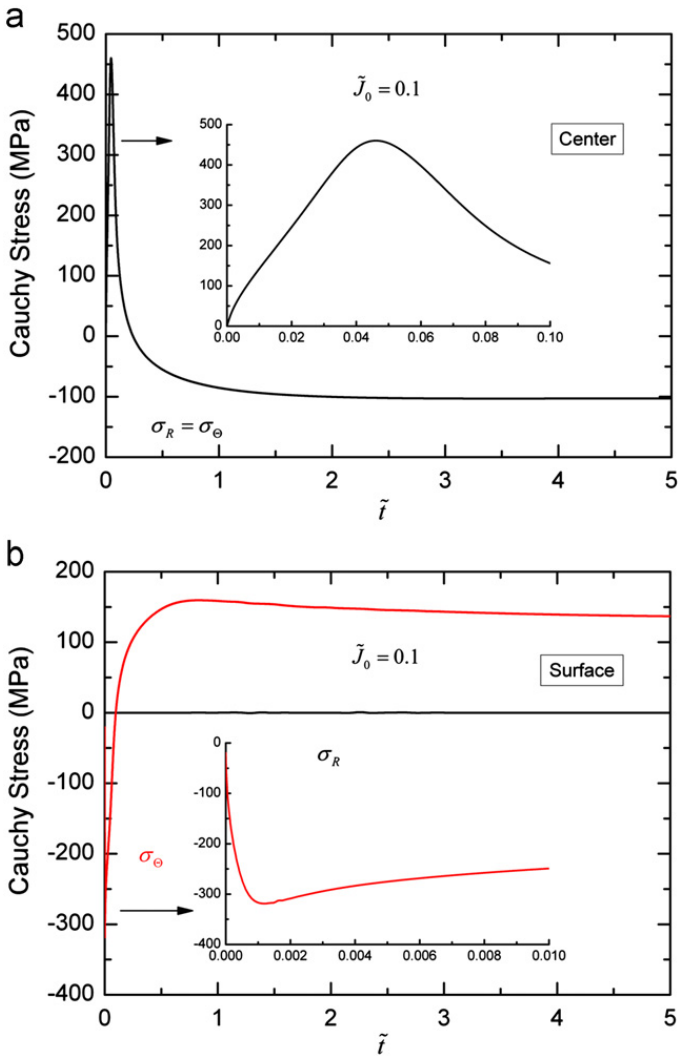

Fig. 11. Evolution of hoop stress at the particle (a) center and (b) surface under different charging rates. The insets are to show the behavior at short charging time.

stress increases (negatively) first, reaches a (negative) maximum, then starts to increase and eventually becomes positive increases with charging time. As pointed out by Zhu (2011), the positive hoop stress near the surface is caused by plasticity. At the very early stage of charging, the surface is subjected to large compressive stress, which causes compressive plastic yielding near the surface. As the charging progresses, the Li concentration near the center of the particle increases. Consequently, the center region starts to expand as well. However, the outer region had already been plastically compressed, which acts as a thin shell that constraints the center region's expansion. As a result, tensile hoop stress is generated near the particle surface. This reverse plasticity might explain the surface cracks observed in the experiments (Ryu et al., 2011; Zhu, 2011).

Another interesting observation is that the center region of the particle remains elastic as shown in Fig. 12 where the distribution of plastic stretch is plotted along the radial direction at several different times. It is seen that the elastic–plastic boundary moves inwardly toward the center of the particle during charging. But, even after a fairly long charging time, the center regions still remains elastic. This is due to the fact that the stress field near the center region is almost hydrostatic (at the center, $\sigma_R = \sigma_\Theta$), which according to the yield criterion used does not facilitate plastic deformation.

The discharging process can be simulated by using the boundary condition given by (36). The corresponding hoop stresses at the center and on the surface are plotted in Fig. 13. On the surface, the hoop stress starts at zero, goes through a maximum compressive stress, and eventually becomes positive. During discharging (Li extraction), the hoop stress on the surface remains positive, and does not return to zero even at fully discharged state. There is clearly residual plastic deformation. At the center, evolution of the hoop stress is similar to the hoop stress on the surface, except the sign is switched. After the second insertion/extraction cycle (not shown), the stress hysteresis becomes stabilized.

In closing, we point out that, although not presented here, we have carried out simulations using several different plastic constitutive laws. It appears that the solutions are very sensitive not only to the type of constitutive laws used, but

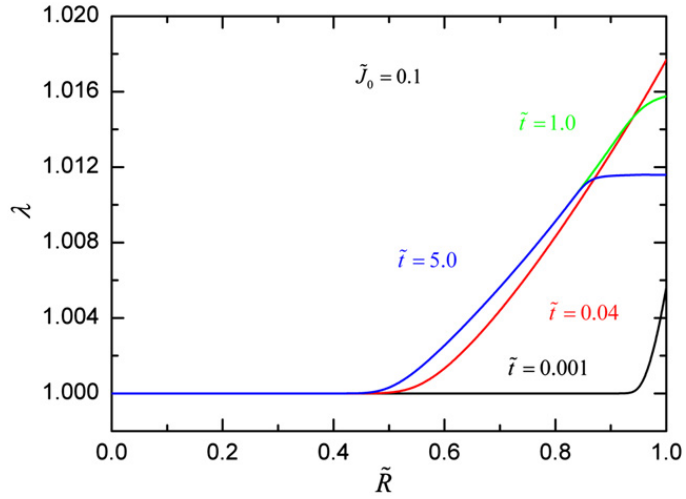

Fig. 12. Distribution of plastic stretch along the radial direction at different times.

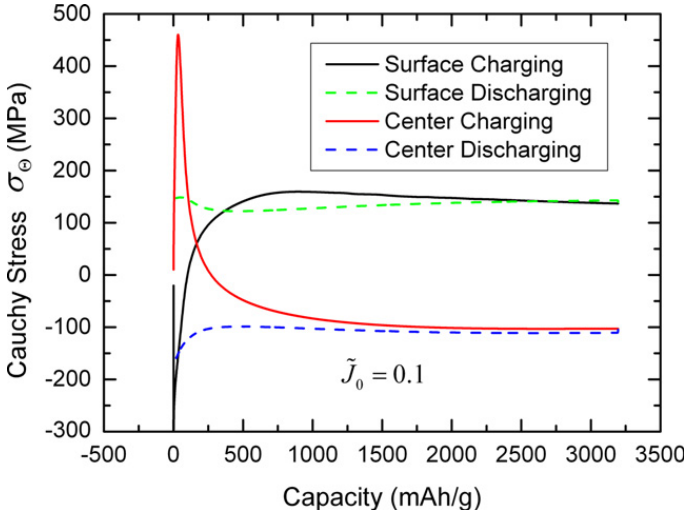

Fig. 13. Evolution of hoop stress on the particle surface and center during the first charging/discharging cycle.

also to the parameters used in these constitutive laws. This points out a critical need to accurately characterize the viscoplastic behavior of Li_xSi alloys either experimentally or through molecular dynamic simulations.

7. Summary

In this paper, an explicit and compact form of the stress-dependent chemical (or diffusion) potential is derived for solids subject to finite strain deformation. The new stress-dependent potential reduces to that of Wu (2001) when the elastic stiffness tensor does not change with the concentration, and to that of Larche and Cahn (1973) when both the elastic and compositional strains are small.

As an example to illustrate the application of this new stress-dependent chemical potential, the stress fields in a spherical amorphous Si particle induced by Li insertion/extraction are investigated in both elastic and elastic–plastic regimes. In the elastic regime, we showed that the critical particle size is inversely related to the insertion rate and scales up as a power law function of the yield strength (see (64)). In the elastic–plastic regime, we found that the hoop stress becomes positive during charging, indicating the particle surface is subjected to tensile hoop stress. We postulated that this tensile hoop stress near the particle surface is responsible for the radial cracks observed in experiments (Ryu et al., 2011; Zhu, 2011). Further, we showed that the center region of the particle remains elastic during the entire Li insertion/extraction cycle.

Acknowledgments

The work is partially supported by a grant from the Initiative of Sustainability and Energy at Northwestern University.

References

Bower, A.F., Guduru, P.R., Sethuraman, V.A., 2011. A finite strain model of stress, diffusion, plastic flow, and electrochemical reactions in a lithium-ion half-cell. J. Mech. Phys. Solids 59, 804–828.

Chen, C.H., Ding, N., Xu, J., Yao, Y.X., Wegner, G., Fang, X., Lieberwirth, I., 2009. Determination of the diffusion coefficient of lithium ions in nano-Si. Solid State Ionics 180 (2–3), 222–225.

Cheng, Y.T., Verbrugge, M.W., 2010. Diffusion-induced stress, interfacial charge transfer, and criteria for avoiding crack initiation of electrode particles. J. Electrochem. Soc. 157 (4), A508–A516.

Cleja-Tigoiu, S., Maugin, G.A., 2000. Eshelby's stress tensors in finite elastoplasticity. Acta Mech. 139, 231–249.

Cui, Z.W., Sun, Y., Chen, Y.J., Qu, J.M., 2011. Semi-ab initio interionic potential for gadolinia-doped ceria. Solid State Ionics 187 (1), 8–18.

Eshelby, J.D., 1951. The force on an elastic singularity. Philos. Trans. R. Soc. London A-Math. Phys. Sci. 244 (877), 87–112.

Eshelby, J.D., 1975. Elastic energy-momentum tensor. J. Elasticity 5 (3–4), 321–335.

Gao, Y.F., Zhou, M., 2011. Strong stress-enhanced diffusion in amorphous lithium alloy nanowire electrodes. J. Appl. Phys. 109 (1), 014310.

Gibbs, J.W., 1906. The Scientific Papers of J. Willard Gibbs. Dover, New York.

Haftbaradaran, H., Song, J., Curtin, W.A., Gao, H.J., 2011. Continuum and atomistic models of strongly coupled diffusion, stress, and solute concentration. J. Power Sources 196 (1), 361–370.

Huang, S., Zhu, T., 2011. Atomistic mechanisms of lithium insertion in amorphous silicon. J. Power Sources 196, 3664–3668.

Kim, H., Chou, C.Y., Ekerdt, J.G., Hwang, G.S., 2011. Structure and properties of Li–Si alloys: a first-principles study. J. Phys. Chem. C 115 (5), 2514–2521.

Larche, F., Cahn, J.W., 1973. Linear theory of thermochemical equilibrium of solids under stress. Acta Metall. 21 (8), 1051–1063.

Larche, F., Cahn, J.W., 1978. Non-linear theory of thermochemical equilibrium of solids under stress. Acta Metall. 26 (1), 53–60.

Larche, F.C., Cahn, J.W., 1982. The effect of self-stress on diffusion in solids. Acta Metall. 30 (10), 1835–1845.

Larche, F.C., Cahn, J.W., 1985. The interactions of composition and stress in crystalline solids. Acta Metall. 33 (3), 331–357.

Larche, F.C., Cahn, J.W., 1987. Stress effects on III–V solid–liquid equilibria. J. Appl. Phys. 62 (4), 1232–1239.

Larche, F.C., Cahn, J.W., 1992. Phase-changes in a thin plate with nonlocal self-stress effects. Acta Metall. 40 (5), 947–955.

Li, J.C.M., Oriani, R.A., Darken, L.S., 1966. Thermodynamics of stressed solids. Z. Phys. Chem.-Frankfurt 49 (3–5), 271.

Liu, X.H., Zheng, H., Zhong, L., Huan, S., Karki, K., Zhang, L.Q., Liu, Y., Kushima, A., Liang, W.T., Wang, J.W., Cho, J.H., Epstein, E., Dayeh, S.A., Picraux, S.T., Zhu, T., Li, J., Sullivan, J.P., Cumings, J., Wang, C.S., Mao, S.X., Ye, Z.Z., Zhang, S.L., Huang, J.Y., 2011. Anisotropic swelling and fracture of silicon nanowires during lithiation. Nano Lett. 11 (8), 3312–3318.

Rhodes, K., Dudney, N., Lara-Curzio, E., Daniel, C., 2010. Understanding the degradation of silicon electrodes for lithium-ion batteries using acoustic emission. J. Electrochem. Soc. 157 (12), A1354–A1360.

Ryu, I., Choi, J.W., Cui, Y., Nix, W.D., 2011. Size-dependent fracture of Si nanowire battery anodes. J. Mech. Phys. Solids 59, 1717.

Sethuraman, V.A., Srinivasan, V., Bower, A.F., Guduru, P.R., 2010. In situ measurements of stress-potential coupling in lithiated silicon. J. Electrochem. Soc. 157 (11), A1253–A1261.

Shenoy, V.B., Johari, P., Qi, Y., 2010. Elastic softening of amorphous and crystalline Li–Si phases with increasing Li concentration: a first-principles study. J. Power Sources 195 (19), 6825–6830.

Swaminathan, N., Qu, J., 2007a. Interactions between non-stoichiometric stresses and defect transport in a tubular electrolyte. Fuel Cells 7 (6), 453–462.

Swaminathan, N., Qu, J., 2009. Evaluation of thermomechanical properties of non-stoichiometric gadolinium doped ceria using atomistic simulations. Model. Simul. Mater. Sci. Eng. 17 (4), 045006.

Swaminathan, N., Qu, J., Sun, Y., 2007b. An electrochemomechanical theory of defects in ionic solids. I. Theory. Philos. Mag. 87 (11), 1705–1721.

Swaminathan, N., Qu, J., Sun, Y., 2007c. An electrochemomechanical theory of defects in ionic solids. Part II. Examples. Philos. Mag. 87 (11), 1723–1742.

Teki, R., Datta, M.K., Krishnan, R., Parker, T.C., Lu, T.M., Kumta, P.N., Koratkar, N., 2009. Nanostructured silicon anodes for lithium ion rechargeable batteries. Small 5 (20), 2236–2242.

Wu, C.H., 2001. The role of Eshelby stress in composition-generated and stress-assisted diffusion. J. Mech. Phys. Solids 49 (8), 1771–1794.

Zhao, K.J., Pharr, M., Cai, S.Q., Vlassak, J.J., Suo, Z.G., 2011a. Large plastic deformation in high-capacity lithium-ion batteries caused by charge and discharge. J. Am. Ceram. Soc. 94, S226–S235.

Zhao, K.J., Pharr, M., Vlassak, J.J., Suo, Z.G., 2011b. Inelastic hosts as electrodes for high-capacity lithium-ion batteries. J. Appl. Phys. 109 (1), 016110.

Zhou, H.G., Qu, J., Cherkaoui, M., 2010a. Finite element analysis of oxidation induced metal depletion at oxide–metal interface. Comput. Mater. Sci. 48 (4), 842–847.

Zhou, H.G., Qu, J., Cherkaoui, M., 2010b. Stress–oxidation interaction in selective oxidation of Cr–Fe alloys. Mech. Mater. 42 (1), 63–71.

Zhu, T., 2011. Private Communication.